
Molecular topological deep learning for polymer property prediction

Cong Shen¹, Yipeng Zhang², Fei Han¹ and Kelin Xia^{2,*}

¹ Department of Mathematics, National University of Singapore, Singapore, 119076, Singapore

² School of Physical and Mathematical Sciences, Nanyang Technological University, Singapore, 637371, Singapore

* Corresponding author

cshen@nus.edu.sg, yipeng001@e.ntu.edu.sg, mathanf@nus.edu.sg,
xiakelin@ntu.edu.sg

Abstract

Accurate and efficient prediction of polymer properties is of key importance for polymer design. Traditional experimental tools and density function theory (DFT)-based simulations for polymer property evaluation, are both expensive and time-consuming. Recently, a gigantic amount of graph-based molecular models have emerged and demonstrated huge potential in molecular data analysis. Even with the great progresses, these models tend to ignore the high-order and multiscale information within the data. In this paper, we develop molecular topological deep learning (Mol-TDL) for polymer property analysis. Our Mol-TDL incorporates both high-order interactions and multiscale properties into topological deep learning architecture. The key idea is to represent polymer molecules as a series of simplicial complexes at different scales and build up simplicial neural networks accordingly. The aggregated information from different scales provides a more accurate prediction of polymer molecular properties.

1 Introduction

Polymers are indispensable for our daily life and continues to drive innovation across industries, from packaging to healthcare and beyond [1, 2]. The development of functional polymers has promoted the usage of polymers to a new level, that is not only within industrial and agricultural production, but goes beyond to healthcare, i.e., treating cancer and genetic diseases [3, 4]. Advanced polymer design and discovery will be the solutions to long-time problems in food, energy, environment, resources and other fields. Polymer informatics [5–7] is to study polymer properties computational tools. Its combination with artificial intelligence (AI) models has demonstrated great potential in polymer property predictors [8–16].

Polymer AI models can be classified into two general types, i.e., fingerprint-based machine learning [17–19] and end-to-end deep learning [20, 21]. The first type is to represent chemical structures and physical properties as fingerprints/descriptors, which are then combined with machine learning models, such as random forest, gradient boosting tree, neural network, etc [17–19]. This type of model is effective and very suitable for small or median-sized dataset. The second type is deep learning models, which are free from handcraft features. In particular, the combination of sequence representations, for instance, simplified molecular-input line-entry system (SMILES), with deep learning models, such as BERT [22], RoBERTa [23], GPT [24], ELMo [25] and XLM [26], has begun to show enormous power [20, 21]. The Transformer model and its variants have been used to predict the properties of polymers. Among them are TransPolymer [21] and polyBERT [20], which use Transformer and BERT models respectively to analyze polymer SMILES sequence

information. Further, geometric deep learning models, in particular Graph Neural Networks (GNNs), have significantly improved the prediction of polymer properties by capturing molecular spatial structure information [22–26, 20, 21, 27–32, 10, 33].

More recently, topological deep learning (TDL) has been proposed a promising tool for analyzing data with complicated topological structures [34–36]. Different from traditional graph neural networks, TDL employs special data representations, including hypergraph, simplicial complexes, cellular complexes, and combinatorial complex, and novel message-passing modules (between simplices of same/different dimensions) [37, 38]. It shows huge potential in the characterization of more complex molecular structures and interactions, and for a better prediction of molecular properties [39–43].

Inspired by TDL, we propose molecular topological deep learning (Mol-TDL) for polymer property prediction. Mol-TDL models the polymer monomer molecule by a series of simplicial complexes at different scales (through a filtration process), which characterize both higher-order and multiscale interactions within the data. For each simplicial complex generated at a particular scale, a simplicial neural network is employed. These simplicial neural networks from different scales, for the same polymer monomer molecule, are then aggregated together for the prediction of polymer property. Further, we develop a multiscale topological contrastive learning model and use it for (self-supervised) pre-training of simplex based message passing. It has been shown that our Mol-TDL model can achieve the-state-of-the-art in predicting polymer properties on well-established benchmark datasets.

2 Related Works

2.1 Graph-based models for polymer property prediction

Graph-based models have been proven to be efficient and powerful in capturing molecular structure information and predicting molecular properties. Especially, the development of graph neural networks has enabled researchers to obtain more effective molecular representations and greatly improve the performance of molecular property prediction. Among them, GEM [27], Mol-GDL [28], HM-GNN [29], KCL [30] and MolCLR [31] are typical representatives of using GNNs to predict molecular properties. Recently, GNNs have been used for the polymer data analysis. For instance, Graph Convolutional Neural Networks (GCNN) has been used in the prediction of dielectric constant and energy bandgap of polymers [32]. The wDMPNN model uses graph-based representation of polymer structure and weighted directed message passing architecture for polymer property prediction [10]. polyGNN combines graph neural network, multitask learning and other advanced deep learning techniques for predicting polymers property [33].

2.2 TDL-based models

Topological Deep Learning (TDL) [34, 35] leverages novel topological tools to characterize data with complicated higher-order structures. Different from graph-based data representation, TDL uses topological representations from algebraic topology, including cell complexes [36, 39, 40], simplicial complexes [35, 44], sheaves [45, 46], combinatorial complexes [34], and hypergraphs [41–43], to model not only pair-wise interactions (as in graphs), but also many-body or higher-order interactions among three or more elements. In fact, these algebraic topology-based molecular representations have already achieved great success in molecular data analysis, including protein flexibility and dynamic analysis [47, 48], drug design [49], virus analysis [50], materials property analysis [51, 52]. Further, TDL uses a generalized message-passing mechanism thus enables the communication of information from simplices of different dimensions. In contrast to GNNs, where information is passing among nodes or edges, TDL allows information to propagate through any neighborhood relation [36, 53, 35, 34, 54].

3 Methods

3.1 Multiscale topological representation for polymer molecule

3.1.1 Simplicial complex representation for polymer molecule

A simplicial complex is the generalization of a graph into its higher-dimensional counterpart. The simplicial complex is composed of simplexes. Each simplex is a finite set of vertices and can

be viewed geometrically as a point (0-simplex), an edge (1-simplex), a triangle (2-simplex), a tetrahedron (3-simplex), and their k -dimensional counterpart (k -simplex). More specifically, a k -simplex $\sigma^k = \{v_0, v_1, v_2, \dots, v_k\}$ is the convex hull formed by $k + 1$ affinely independent points $v_0, v_1, v_2, \dots, v_k$ as follows

$$\sigma^k = \left\{ \lambda_0 v_0 + \lambda_1 v_1 + \dots + \lambda_k v_k \mid \sum_{i=0}^k \lambda_i = 1; \forall i, 0 \leq \lambda_i \leq 1 \right\}.$$

The i th dimensional face of σ^k ($i < k$) is the convex hull formed by $i + 1$ vertices from the set of $k + 1$ points $v_0, v_1, v_2, \dots, v_k$. The simplexes are the basic components for a simplicial complex.

A simplicial complex K is a finite set of simplexes that satisfy two conditions. First, any face of a simplex from K is also in K . Second, the intersection of any two simplexes in K is either empty or a shared face. A k th chain group C_k is an Abelian group of oriented k -simplexes σ^k , which are simplexes together with an orientation, i.e., ordering of their vertex set. The boundary operator $\partial_k(C_k \rightarrow C_{k-1})$ for an oriented k -simplex σ^k can be denoted as

$$\partial_k \sigma^k = \sum_{i=0}^k (-1)^i [v_0, v_1, v_2, \dots, \hat{v}_i, \dots, v_k].$$

Here, $[v_0, v_1, v_2, \dots, \hat{v}_i, \dots, v_k]$ is an oriented $(k - 1)$ -simplex, which is generated by the original set of vertices except v_i . The boundary operator maps a simplex to its faces, and it guarantees that $\partial_{k-1} \partial_k = 0$. To facilitate a better description, we use notation $\sigma_j^{k-1} \subset \sigma_i^k$ to indicate that σ_j^{k-1} is a face of σ_i^k . For two oriented k -simplexes, σ_i^k and σ_j^k , of a simplicial complex K , they are upper adjacent, denoted as $\sigma_i^k \frown \sigma_j^k$, if they are faces of a common $(k + 1)$ -simplex; they are lower adjacent, denoted as $\sigma_i^k \smile \sigma_j^k$, if they share a common $(k - 1)$ -simplex as their face. The upper degree of a k -simplex σ_i^k , denoted as $d_U(\sigma_i^k)$, is the number of $(k + 1)$ -simplexes, of which σ_i^k is a face. Similarly, we define the lower degree of σ_i^k , denoted as $d_L(\sigma_i^k)$, to be the number of $(k - 1)$ -simplexes on the boundary of σ_i^k .

3.1.2 Filtration-based multiscale representation

A filtration process naturally generates a multiscale representation [55]. The filtration parameter, which is key to the filtration process, is usually chosen as sphere radius (or diameter) for point cloud data, edge weight for graphs, and isovalue (or level set value) for density data. A systematical increase (or decrease) of the value for the filtration parameter will induce a sequence of hierarchical topological representations, which can be not only simplicial complexes but also graphs and hypergraphs. For instance, a filtration operation on a distance matrix, i.e., a matrix with distances between any two vertices as its entries, can be defined by using a cutoff value as the filtration parameter. More specifically, if the distance between two vertices is smaller than the cutoff value, an edge is formed between them. In this way, a systematical increase (or decrease) of the cutoff value will deliver a series of nested graphs, with the graph produced at a lower cutoff value as a part (or a subset) of the graph produced at a larger cutoff value. Similarly, nested simplicial complexes can be constructed by using various definitions of complexes, such as Vietoris-Rips complex, Čech complex, alpha complex, cubical complex, Morse complex, and clique complex. In this study, we employ the Vietoris-Rips complex to describe both the topological and geometric structure of a given point cloud. Formally, the Vietoris-Rips complex, denoted as $\text{Rip}_r = \text{Rip}_r(X)$, is defined for a point cloud X and a cutoff value r , as follows:

$$\text{Rip}_r(X) := \{ \sigma \subseteq X \mid \sigma \text{ is finite and } \forall \mathbf{x}_i, \mathbf{x}_j \in \sigma, \|\mathbf{x}_i - \mathbf{x}_j\| \leq r \},$$

where σ represents a simplex in X , and $\|\mathbf{x}_i - \mathbf{x}_j\|$ denotes the Euclidean distance between any two points \mathbf{x}_i and \mathbf{x}_j in σ .

In Mol-TDL, pairwise distance between atoms is corresponding to the cutoff value r in Vietoris-Rips complex Rip_r . Given the significance of actual inter-atomic distances in our study, we set the parameter r to span from 2.0 to 4.0 Å. To facilitate discretization within this range, we consider five distinct Vietoris-Rips complexes Rip_r , for $r = 2.0, 2.5, 3.0, 3.5,$ and 4.0 Å in our model. Figure 1 A shows an example of the filtration-based multiscale representation for a molecule.

In the previous section, we discussed two k -simplex relations in a simplicial complex: the upper adjacency and lower adjacency relations. In this section, we consider these relations as interactions between k -simplexes within the mentioned Vietoris-Rips complexes Rip_r . Specifically, we focus on the upper adjacency relation for all 0-simplexes. This means an interaction occurs between two atoms if and only if their distance does not exceed r . This interaction is the same the traditional understanding of molecular graph interactions. When considering higher-order k -simplexes (where $k > 0$), we consider their lower adjacency; that is, two k -simplexes interact if and only if their common face is a $(k - 1)$ -simplex. We use adjacency matrix $A_{r,k} = \{A_{r,k}(i, j)\}$ to describe this interaction between k -simplexes in Rip_r :

$$A_{r,0}(i, j) = \begin{cases} 1, & \sigma_i^{r,0} \frown \sigma_j^{r,0}, i \neq j \\ 0, & \text{others.} \end{cases}$$

And for $k \geq 1$:

$$A_{r,k}(i, j) = \begin{cases} 1, & \sigma_i^{r,k} \smile \sigma_j^{r,k}, i \neq j \\ 0, & \text{others.} \end{cases}$$

where $\sigma_i^{r,k}$ is the i -th k -simplex in Rip_r . And the notation \frown and \smile represent the upper and lower adjacency relation, respectively.

Also we consider the following diagonal matrices $D_{r,k} = \{D_{r,k}(i, j)\}$ for normalization:

$$D_{r,0}(i, j) = \begin{cases} d_U(\sigma_i^{r,0}), & i = j \\ 0, & \text{others.} \end{cases}$$

And for $k \geq 1$:

$$D_{r,k}(i, j) = \begin{cases} d_L(\sigma_i^{r,k}), & i = j \\ 0, & \text{others.} \end{cases}$$

where $d_U(\sigma_i^{r,k})$ and $d_L(\sigma_i^{r,k})$ denote the upper and lower degree of $\sigma_i^{r,k}$, respectively.

3.2 Multiscale topological deep learning

3.2.1 Simplex-based message passing

In Mol-TDL, Vietoris-Rips complexes Rip_r is utilized to describe polymer. To be specific, we consider a series of adjacent matrices $A_{r,k}$ to describe the interaction between k -simplexes in Rip_r . We use message passing to learn the feature representation of each simplex,

$$H_{r,k}^{(l+1)} = \text{Relu} \left(\hat{D}_{r,k}^{-\frac{1}{2}} \hat{A}_{r,k} \hat{D}_{r,k}^{-\frac{1}{2}} H_{r,k}^{(l)} W_{r,k}^{(l)} \right). \quad (1)$$

In the l -th iteration, the feature matrix $H_{r,k}^{(l+1)}$ of k -simplexes is obtained by gathering neighbors feature of each k -simplex. Here $\hat{A}_{r,k}$ represents the sum of $A_{r,k}$ and identity matrix. $\hat{D}_{r,k}$ is a degree matrix, which is a diagonal matrix whose values on the diagonal are equal to the sum of the corresponding rows (or columns) in $\hat{A}_{r,k}$. $W_{r,k}^{(l)}$ is the weight matrix (to be learned). Computationally, we usually repeat the process 1 to 3 times, and the final simplex feature is denoted as $H_{r,k}$.

After message passing, the feature $H_{r,k}$ of k -simplex and its initial feature $H_{r,k}^{(0)}$ are concatenated together, and then all k -simplex features in Rip_r are gathered into one feature through a pooling process,

$$f_{r,k} = \text{Pooling} \left([H_{r,k} \parallel H_{r,k}^{(0)}] \right),$$

where $\text{Pooling}(\cdot)$ is a pooling function applied to all row vectors of the matrix and $[\cdot \parallel \cdot]$ is concatenation operation.

In Mol-TDL, we consider five the filtration values. In this step, all features of k -simplexes in different filtration values are aggregated,

$$f_k = \text{READOUT}_1 (f_{r,k} | r = 2.0, 2.5, \dots, 4.0).$$

Then all features in different orders are systematically aggregated,

$$f = \text{READOUT}_2 (f_k \mid k = 0, 1, 2),$$

where $\text{READOUT}_1(\cdot)$ and $\text{READOUT}_2(\cdot)$ both denote pooling function, and we choose concatenation in this study. Here f is the final representation of a polymer.

Finally, a multiply layer perceptron (MLP) is utilized to property prediction,

$$\hat{y} = W^1 \text{Relu} (W^0 f + b^0) + b^1,$$

where W^0 and W^1 are weight matrix, and b^0 and b^1 are the bias. The ℓ_1 loss is implemented for regression tasks in Mol-TDL. Figure 1B illustrates the flowchart of our Mol-TDL.

3.2.2 Multiscale representation from simplex messages

The initialization features of the k -simplex are crucial for predicting the properties of the polymer. Since the geometric meanings of k -simplex are obviously different, in Mol-TDL, different types of simplex have different feature initialization method.

For 0-simplex, which represents atom in a molecule, we refer Mol-GDL [28] and consider a total of 12 types of atoms, including C, H, O, N, P, Cl, F, Br, S, Si, I and all the rest atoms as one type. These atoms are chosen due to their high frequencies in the molecules in our datasets. For the i -th atom, atom type a_j will contribute a component $g_i(r, \alpha_j)$ in the geometric node feature $g_i(r) = [g_i(r, \alpha_1), g_i(r, \alpha_2), \dots, g_i(r, \alpha_{12})]$. Here $g_i(r, \alpha_j)$ means the number (or frequency) of all the neighboring atoms of type α_j for the i -th atom. For more details, please refer to Mol-GDL [28].

For 1-simplex, which represents a bond in a molecule, we take the distance information as its initial features and use radial basis functions (RBF) [56] to represent this feature $g_{\text{RBF}}(d, \varepsilon, c) = e^{-\varepsilon \|d-c\|^2}$, where d is distance between two nodes in a 1-simplex. Here, ε is a hyper-parameter and we set $\varepsilon = 1$. c is center node and its value is chosen from $\{0, 0.1, 0.2, \dots, 0.9\}$. Thus, a 10-dimensional initial feature vector, $[g_{\text{RBF}}(d, 1, c) \mid c = 0, 0.1, 0.2, \dots, 0.9]$ of 1-simplex can be obtained after inputting a distance value d .

For 2-simplex, which represents a triangle within a molecule, we take into account geometric information including area of the triangle, three related angles, and gravity center of the triangle. First, Heron’s formula is used to calculate the area of the triangle, $g_{\text{area}} = \sqrt{p(p - e_1)(p - e_2)(p - e_3)}$, where e_1, e_2 and e_3 represent the length of three edges, respectively. p is half the circumference of a triangle, that is $p = \frac{1}{2}(e_1 + e_2 + e_3)$. Then, the cosines of the three angles in the triangle is utilized as the second part of the 2-simplex initial feature, that is \cos_1, \cos_2 and \cos_3 . Next, the center of gravity of the triangle is calculated by averaging three atom coordinates, denoted as $\text{cen}_1, \text{cen}_2$ and cen_3 . Finally, all of this geometric information is concatenated to form a 7-dimensional initial feature of the 2-simplex, which is $[g_{\text{area}}, \cos_1, \cos_2, \cos_3, \text{cen}_1, \text{cen}_2, \text{cen}_3]$.

3.3 Multiscale topological contrastive learning

Motivated by recent developments in contrastive learning models for molecular property prediction [31, 30, 57], we develop a multiscale topological contrastive learning for (self-supervised) pre-training of simplex-based message passing. In topological contrastive learning, pre-training is performed through maximizing the agreement between two augmented views of the same simplicial complex via a contrastive loss in the latent space. The framework consists of the following four major components:

(1) **Topological data augmentation.** In graph models, graph data augmentation methods include node dropping, edge perturbation, attribute masking and subgraph sampling [58]. In our Mol-TDL model, we introduce simplex-based attribute masking, which is to mask part of (initial) simplex features to augment the data. For a given polymer, it can be represented as a series of Rip_r , which undergo topological data augmentations to obtain two correlated views $H_{r,k}^a$ and $H_{r,k}^b$. Here $H_{r,k}^a$ represents original initial features of the k -simplex at cutoff distance r , and $H_{r,k}^b$ is generated by attribute masking. More specifically, we replace 30% of the elements in the initial simplex features with random values. In contrastive learning, the pair of $H_{r,k}^a$ and $H_{r,k}^b$ forms a positive pair.

In our simplicial complex contrastive framework, the augmented views are utilized for a downstream task of label prediction. Inspired by the work[59], we define the optimality of the views based on

the mutual information. The main idea is that the optimal augmented views should retain all the information from the input simplicial complex relevant to the label, and all the shared information between the views should only be task-relevant.

Proposition 1. (Optimal Augmented Views) For a downstream task T of prediction of a semantic label y , the optimal views, $(H_{r,k}^a)^*$, $(H_{r,k}^b)^*$, generated from the input simplicial complex Rip_r are the solutions to the following optimization problem:

$$(v_1^*, v_2^*) = \arg \min_{v_1, v_2} I(v_1; v_2) \quad (2)$$

subject to

$$I(v_1; y) = I(v_2; y) = I(\text{Rip}_r; y), \quad (3)$$

Here $I(X; Y) := \mathbb{E}_{p(x,y)} \left[\log \frac{p(x,y)}{p(x)p(y)} \right]$ denotes the mutual information of random variables X, Y ; $p(x, y)$ is the joint probability density function of X, Y and $p(x), p(y)$ are the marginal probability density functions of X and Y respectively. Proposition 1 reveals that the shared information shared between the optimal views is minimized (Equation (2)). The proof of this proposition is in the Appendix.

(2) **Simplex-based message passing encoder.** A simplex-based message passing encoder (defined in Section 3.2.1) extracts simplicial complex representation vectors f^a and f^b as in Equation (4) for augmented simplicial complex pairs $H_{r,k}^a$ and $H_{r,k}^b$.

(3) **Contrastive loss function.** A contrastive loss function $\mathcal{L}(\cdot)$ is defined to enforce maximizing the consistency between positive pairs f^a and f^b compared with negative pairs. Here the normalized temperature-scaled cross entropy loss [60, 61] is utilized to calculate contrastive loss.

During pre-training of simplex-based message passing, a minibatch of M_{batch} polymer data are randomly sampled and processed through contrastive learning, resulting in $2M_{batch}$ augmented polymer data and corresponding contrastive loss to optimize, where we denote j -th polymer data pair as f_j^a and f_j^b in the minibatch. Negative pairs are not explicitly sampled but generated from the other $2M_{batch} - 1$ augmented polymer data within the same minibatch as in [62]. Denoting the cosine similarity function as,

$$sim(f_j^a, f_j^b) = \frac{(f_j^a)^T f_j^b}{\|f_j^a\| \|f_j^b\|}. \quad (4)$$

The normalized temperature-scaled cross entropy loss [60, 61] for the j -th positive pair is defined as:

$$\mathcal{L}(f_j^a, f_j^b) = -\log \left(\frac{\exp(sim(f_j^a, f_j^b) / \tau)}{\sum_{j' \neq j}^{M_{batch}} \exp(sim(f_j^a, f_{j'}^b) / \tau)} \right),$$

where τ denotes the temperature parameter. The final loss is computed across all positive pairs in the minibatch, i.e., $\sum_j \mathcal{L}(f_j^a, f_j^b)$.

4 Results

4.1 Performance of Mol-TDL for polymer property prediction

In this section, we present the comparison results between our Mol-TDL and SOTAs on different types of polymer data analysis. These datasets can be roughly classified into three categories: Electronic (E_{gc} [8], E_{gb} [8], E_{ea} [8], E_i [8], $E_{gap}^{crystal}$ [63], E_{gap}^{chain} [63], Φ_e^{BC} [63], OPV_{Ave} [64], OPV_{Jsc} [64], OPV_{Voc} [64], OPV_{Eg} [64], OPV_{HOMO} [64], OPV_{LUMO} [64], Optical & dielectric(ϵ_0 [8], n_c [8]) and Thermodynamic & physical(X_c [8]). For these datasets, we only use their repeat unit, i.e. monomers, to construct simplicial complexes and predict its performance. The detailed information of datasets can be found in Appendix Table 1. All datasets of Mol-TDL model are split by ratio 8:1:1 for training, validation and test sets randomly.

For benchmarking, the performance of Mol-TDL is compared with five state-of-the-art polymer/molecular property prediction models: polyBERT [20], TransPolymer [7], polyGNN [33], Mol-GDL [28] and GEM [27]. Here, Root Mean Square Error (RMSE) and R^2 are used as metrics

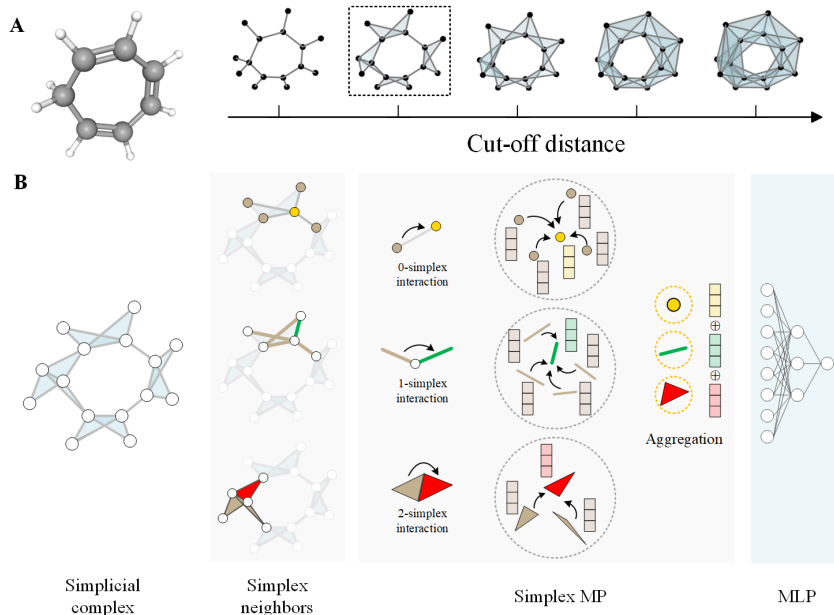


Figure 1: Flowchart of Mol-TDL model. **A** Filtration of the Vietoris–Rips Complex for Cycloheptatriene. The Vietoris–Rips complex is applied at various cut-off distances: 2.0, 2.5, 3.0, 3.5, and 4.0 Å in our model. **B** Topological deep learning model which utilizes a simplicial complex derived from the Vietoris–Rips complex with a cut-off distance. The neighborhood structure is constructed through interactions among 0, 1, and 2-simplexes. Message Passing (MP) in the model is implemented based on this neighborhood structure, followed by pooling operation and a Multilayer Perceptron (MLP) for regression analysis.

for evaluation in Mol-TDL and all benchmark. It is worth noting that we directly use the original results if the baseline model has RMSE and R^2 in the original literature, otherwise, we obtain the experimental results by running the code provided by the original literature.

Table 1 shows that Mol-TDL can achieve good prediction performance on most data sets. Appendix Figure 1 and 2 show the comparison between the predicted property with the density functional theory (DFT). Although the prediction models polyBERT and TransPolymer based on sequence information have larger-scale pre-training (polyBERT uses 100 million PSMILES strings, and TransPolymer uses 5 million augmented data for pre-training), Mol-TDL still has a competitive advantage even with a small pre-training scale. This shows that Mol-TDL has a more powerful advantage in capturing the spatial structure and topological information of polymers from the simplicial complex level. Compared with the classic models GEM and Mol-GDL used for molecular property prediction, Mol-TDL can still achieve prediction performance that is not inferior to these two models. GEM takes into account the correlation of higher-order interaction and other geometric information, like angles, but this model only learns its spatial structure information on the covalent bond molecular graph, while ignoring non-covalent bond information. Although the Mol-GDL model takes into account non-covalent bond information, it lacks more attention to high-order interaction and the geometric quantities in non-covalent bond information. Therefore, the performance of Mol-GDL in polymer property prediction is also inferior to Mol-TDL.

In order to further verify the Mol-TDL’s representation ability for polymers, we compared the learned latent representations/spaces from Mol-TDL and polyBERT models. First, we visualize the pre-trained representations to verify whether they capture the scaffold information [65], which is used to represent the core structures of bioactive compounds. Intuitively, molecules with the same scaffold share similar structure, and therefore are expected to be close in the high-level representation space. We randomly select four scaffolds and sample 100 molecules for each scaffold. Then we extract features of these molecules using Mol-TDL and polyBERT model. The t -distributed stochastic neighbor embedding (t -SNE) is used to reduce the dimensionality of the extracted features and visualize them into a 2D space. As shown in Appendix Figure 3A, it is not difficult to find that

Table 1: Performance of Mol-TDL and baseline models. (Note that * represents the results come from the original article, and N/A represents that the SMILES does not meet the model input specifications and no results can be obtained)

	polyBERT	TransPolymer	polyGNN	Mol-GDL	GEM	Mol-TDL
Metrics: R^2						
E_{gc}	0.89 \pm 0.02	0.92 \pm 0.00	0.916 \pm 0.005	0.869 \pm 0.004	0.713 \pm 0.018	0.881 \pm 0.006
E_{gb}	0.93 \pm 0.01	0.93 \pm 0.01	0.839 \pm 0.067	0.921 \pm 0.005	0.860 \pm 0.022	0.936 \pm 0.005
E_{ea}	0.93 \pm 0.03	0.91 \pm 0.03	0.781 \pm 0.108	0.596 \pm 0.058	0.909 \pm 0.032	0.944 \pm 0.005
E_i	0.82 \pm 0.07	0.84 \pm 0.06	0.786 \pm 0.156	0.758 \pm 0.021	0.660 \pm 0.035	0.867 \pm 0.013
X_c	0.349 \pm 0.016	0.50 \pm 0.06	0.397 \pm 0.073	0.421 \pm 0.052	0.406 \pm 0.093	0.579 \pm 0.045
ε_0	0.724 \pm 0.012	0.76 \pm 0.11	0.354 \pm 0.404	0.716 \pm 0.032	0.790 \pm 0.043	0.801 \pm 0.019
n_c	0.86 \pm 0.06	0.82 \pm 0.07	0.543 \pm 0.307	0.851 \pm 0.012	0.828 \pm 0.073	0.882 \pm 0.021
$E_{gap}^{crystal}$	0.829 \pm 0.005	0.750 \pm 0.018	N/A	0.819 \pm 0.044	0.787 \pm 0.135	0.899 \pm 0.020
E_{gap}^{chain}	0.782 \pm 0.004	0.861 \pm 0.009	N/A	0.844 \pm 0.007	0.606 \pm 0.031	0.863 \pm 0.006
Φ_e^{BC}	0.650 \pm 0.013	0.755 \pm 0.006	N/A	0.703 \pm 0.019	0.759 \pm 0.039	0.749 \pm 0.014
OPV_{Ave}	0.299 \pm 0.003	0.32 \pm 0.05	N/A	0.350 \pm 0.011	0.256 \pm 0.022	0.357 \pm 0.022
OPV_{Jsc}	0.294 \pm 0.009	0.354 \pm 0.023	N/A	0.215 \pm 0.016	0.194 \pm 0.045	0.262 \pm 0.028
OPV_{Voc}	0.241 \pm 0.021	0.274 \pm 0.019	N/A	0.329 \pm 0.038	0.305 \pm 0.015	0.503 \pm 0.043
OPV_{Eg}	0.401 \pm 0.026	0.553 \pm 0.033	N/A	0.569 \pm 0.032	0.356 \pm 0.050	0.468 \pm 0.036
OPV_{HOMO}	0.184 \pm 0.035	0.466 \pm 0.052	N/A	0.401 \pm 0.097	0.375 \pm 0.087	0.379 \pm 0.056
OPV_{LUMO}	0.375 \pm 0.020	0.487 \pm 0.034	N/A	0.471 \pm 0.027	0.133 \pm 0.009	0.514 \pm 0.035
Metrics: $RMSE$						
E_{gc}	0.701 \pm 0.008	0.44 \pm 0.01	0.442 \pm 0.020	0.583 \pm 0.009	0.560 \pm 0.014	0.510 \pm 0.012
E_{gb}	0.567 \pm 0.020	0.52 \pm 0.05	0.540 \pm 0.170	0.553 \pm 0.019	0.534 \pm 0.042	0.485 \pm 0.017
E_{ea}	0.308 \pm 0.004	0.32 \pm 0.02	0.341 \pm 0.055	0.552 \pm 0.596	0.274 \pm 0.050	0.263 \pm 0.013
E_i	0.525 \pm 0.011	0.39 \pm 0.07	0.540 \pm 0.170	0.563 \pm 0.024	0.313 \pm 0.016	0.417 \pm 0.021
X_c	17.646 \pm 0.220	16.57 \pm 0.68	18.6 \pm 1.90	18.768 \pm 0.858	17.820 \pm 1.684	15.862 \pm 0.825
ε_0	0.496 \pm 0.011	0.52 \pm 0.07	0.362 \pm 0.086	0.501 \pm 0.029	0.495 \pm 0.066	0.350 \pm 0.016
n_c	0.131 \pm 0.004	0.10 \pm 0.02	0.093 \pm 0.030	0.086 \pm 0.004	0.092 \pm 0.023	0.068 \pm 0.006
$E_{gap}^{crystal}$	0.613 \pm 0.009	0.741 \pm 0.027	N/A	0.615 \pm 0.071	0.702 \pm 0.174	0.567 \pm 0.057
E_{gap}^{chain}	0.683 \pm 0.007	0.546 \pm 0.018	N/A	0.570 \pm 0.013	0.777 \pm 0.031	0.539 \pm 0.012
Φ_e^{BC}	0.669 \pm 0.013	0.560 \pm 0.006	N/A	0.581 \pm 0.069	0.476 \pm 0.038	0.539 \pm 0.015
OPV_{Ave}	2.015 \pm 0.005	1.92 \pm 0.06	N/A	1.884 \pm 0.016	2.267 \pm 0.033	1.843 \pm 0.031
OPV_{Jsc}	3.378 \pm 0.022	3.231 \pm 0.057	N/A	3.740 \pm 0.038	0.365 \pm 0.025	3.644 \pm 0.069
OPV_{Voc}	0.118 \pm 0.002	0.115 \pm 0.002	N/A	0.129 \pm 0.004	0.111 \pm 0.001	0.104 \pm 0.005
OPV_{Eg}	0.158 \pm 0.003	0.137 \pm 0.005	N/A	0.128 \pm 0.005	0.158 \pm 0.006	0.146 \pm 0.005
OPV_{HOMO}	0.209 \pm 0.008	0.171 \pm 0.008	N/A	0.164 \pm 0.008	0.168 \pm 0.009	0.161 \pm 0.007
OPV_{LUMO}	0.249 \pm 0.004	0.209 \pm 0.007	N/A	0.211 \pm 0.005	0.215 \pm 0.001	0.205 \pm 0.007

Mol-TDL and polyBERT are similar in their t -SNE distributions, where both can cluster different scaffolds well. However, the clustering effect of the Mol-TDL model is better than the polyBERT model on certain scaffold types, such as the scaffold represented by the blue points. Quantitatively, in terms of the Davies Bouldin index (DBI) [66] (the smaller, the better), which is a metric to evaluate the clustering results, Mol-TDL clearly outperforms polyBERT model. Besides, We also randomly select three scaffolds and sample 100 molecules for each scaffold. The result is shown in Appendix Figure 4, and Mol-TDL also has better visualization performance. Another visualize test is that we use t -distributed stochastic neighbor embedding (t -SNE) to directly reduce the representation vectors learned by the Mol-TDL and polyBERT models to 2D space, as shown in Appendix Figure 3B and Appendix Figure 5. Overall, on these data sets, the Mol-TDL model’s representation ability for polymers is significantly better than polyBERT. It is worth noting that on data sets such as E_{gb} , E_{ea} and E_{gap}^{chain} , the advantages of the Mol-TDL model are particularly prominent because points of the same color are more obviously clustered together.

4.2 Ablation study

In Mol-TDL, instead of using only one molecular graph, a series of simplicial complexes are systematically generated by selecting different filtration cutoff value r_i (see Method for details). Here, five filtration cutoff values, $r = 2.0, 2.5, 3.0, 3.5, 4.0 \text{ \AA}$, are chosen to generate the simplicial complexes (Figure 1 A) and three different order simplexes (0-simplex, 1-simplex, 2-simplex) are

chosen for constructed higher-order interactions. The simplicial complex whose chemical bond length is between 0 \AA and 2 \AA is the *de facto* standard of the covalent-bond-based model, and the other four are all constructed using covalent and non-covalent. For instance, a simplicial complex with a cut-off distance of 3 \AA means that the length of all the bond in this simplicial complex k are no more than 3 \AA . Message passing in the model is implemented based on 0, 1, and 2-simplex interactions (See Figure 1 B). For example, when considering 2-simplex interaction, messages are passed between pairs of 2-simplexes that share this type of interaction.

Appendix Figure 6 shows the performance of Mol-TDL models under different cutoff distances and simplicial complices at different dimensions. More specifically, the "0-simplex" model means we only consider TDL based on 0-simplex message passing. The notation of "0,1-simplex" model means that both 0-simplex interactions and 1-simplex interactions are considered, while "0,1,2-simplex" model means that 0-simplex interactions, 1-simplex interactions and 2-simplex interactions are considered simultaneously. It can be seen that the consideration of higher order information can always improve the performance of the model, regardless of the cutoff distances. For both datasets, the performance of model will be enhanced when higher-order simplexes are added. The average values of the models from different cutoff distances are demonstrated in the right side of Appendix Figure 6. The same trend can be observed. Further, non-covalent interactions play an important role in the performance of models. In fact, the best performance is not at the cut-off distance of 2 \AA , which usually indicates covalent interactions. Instead for the ϵ_0 dataset, the model has the best performance with a cut-off distance of 3 \AA , and the performance on the simplicial complexes with a cut-off distance of 3.5 \AA and 4 \AA are also better than that of the simplicial complex with a cut-off distance of 2 \AA . On the E_{gb} data set, it can be seen more clearly that the prediction performance on simplicial complex with a cut-off distance of 2 \AA is worse than the performance on simplicial complexes with the other four higher cut-off distances. The effects of non-covalent bonds and higher-order interactions on model performance in other data sets are shown in Appendix Table 2 to 9.

In order to enable the Mol-TDL model to capture more structural information of polymers and further improve the performance of the model, multiscale topological contrastive learning and large-scale polymer structural data is used to pre-train Mol-TDL. We randomly select 1,000,000 polymers from TransPolymer [7] and set the ratio of the training and validation set is 9:1 to pre-train Mol-TDL. Appendix Table 10 shows the difference in performance of the Mol-TDL model with and without pre-training. It is not difficult to find that the Mol-TDL model with pre-training is better than the Mol-TDL without pre-training as a whole. This result is more obviously reflected in E_{ea} , E_i and X_c . However, it is worth noting that Mol-TDL pre-training does not improve performance on some data sets, such as E_{gb} and E_{gap}^{chain} . We analyzed that the reason is that the amount of pre-training data is too small, and the E_{gap}^{chain} used for fine-tuning are relatively large, so pre-training cannot provide more effective information for these fine-tuning data.

5 Conclusion

Efficient polymer representation learning is crucial for polymer property prediction. Existing works that apply graph neural network methods for polymer property prediction fail to characterize higher-order and multiscale information. To this end, we design molecular topological deep learning (Mol-TDL), which incorporates both high-order interactions and multiscale properties into topological deep learning models. The key idea is to use a series of simplicial complexes at different scales to represent polymer monomer molecule and employ the simplex message-passing modules. In addition, multiscale topological contrastive learning is used to pre-train the model, thereby enriching the structural information of Mol-TDL from large-scale simplicial complexes. Our Mol-TDL model can achieve the state-of-the-art results in polymer benchmark datasets.

Limitations The Mol-TDL model can be further improved by the consideration of coupling of simplex message-passing modules at different dimensions. Currently, the simplex message-passing modules are done individually and lack communication between each other. A more sophisticated simplex message-passing architecture can be employed for more efficient characterization and learning of the high-order and multiscale information.

Acknowledgments and Disclosure of Funding

References

- [1] LaShanda TJ Korley, Thomas H Epps III, Brett A Helms, and Anthony J Ryan. Toward polymer upcycling—adding value and tackling circularity. *Science*, 373(6550):66–69, 2021.
- [2] Geoffrey W Coates and Yutan DYL Getzler. Chemical recycling to monomer for an ideal, circular polymer economy. *Nature Reviews Materials*, 5(7):501–516, 2020.
- [3] Tanmay Banerjee, Filip Podjaski, Julia Kröger, Bishnu P Biswal, and Bettina V Lotsch. Polymer photocatalysts for solar-to-chemical energy conversion. *Nature Reviews Materials*, 6(2):168–190, 2021.
- [4] Joshua C Worch, Hannah Prydderch, Sètuhn Jimaja, Panagiotis Bexis, Matthew L Becker, and Andrew P Dove. Stereochemical enhancement of polymer properties. *Nature Reviews Chemistry*, 3(9):514–535, 2019.
- [5] Rohit Batra, Le Song, and Rampi Ramprasad. Emerging materials intelligence ecosystems propelled by machine learning. *Nature Reviews Materials*, 6(8):655–678, 2021.
- [6] Debra J Audus and Juan J de Pablo. Polymer informatics: Opportunities and challenges. *ACS macro letters*, 6(10):1078–1082, 2017.
- [7] Nico Adams and Peter Murray-Rust. Engineering polymer informatics: towards the computer-aided design of polymers. *Macromolecular rapid communications*, 29(8):615–632, 2008.
- [8] Christopher Kuenneth, Arunkumar Chitteth Rajan, Huan Tran, Lihua Chen, Chiho Kim, and Rampi Ramprasad. Polymer informatics with multi-task learning. *Patterns*, 2(4), 2021.
- [9] Huan Doan Tran, Chiho Kim, Lihua Chen, Anand Chandrasekaran, Rohit Batra, Shruti Venkatram, Deepak Kamal, Jordan P Lightstone, Rishi Gurnani, Pranav Shetty, et al. Machine-learning predictions of polymer properties with polymer genome. *Journal of Applied Physics*, 128(17), 2020.
- [10] Matteo Aldeghi and Connor W Coley. A graph representation of molecular ensembles for polymer property prediction. *Chemical Science*, 13(35):10486–10498, 2022.
- [11] Guang Chen, Lei Tao, and Ying Li. Predicting polymers’ glass transition temperature by a chemical language processing model. *Polymers*, 13(11):1898, 2021.
- [12] J Wesley Barnett, Connor R Bilchak, Yiwen Wang, Brian C Benicewicz, Laura A Murdock, Tristan Bereau, and Sanat K Kumar. Designing exceptional gas-separation polymer membranes using machine learning. *Science advances*, 6(20):eaaz4301, 2020.
- [13] Chiho Kim, Rohit Batra, Lihua Chen, Huan Tran, and Rampi Ramprasad. Polymer design using genetic algorithm and machine learning. *Computational Materials Science*, 186:110067, 2021.
- [14] Joseph Kern, Lihua Chen, Chiho Kim, and Rampi Ramprasad. Design of polymers for energy storage capacitors using machine learning and evolutionary algorithms. *Journal of Materials Science*, 56:19623–19635, 2021.
- [15] Rishi Gurnani, Deepak Kamal, Huan Tran, Harikrishna Sahu, Kenny Scharm, Usman Ashraf, and Rampi Ramprasad. PolyG2G: A novel machine learning algorithm applied to the generative design of polymer dielectrics. *Chemistry of Materials*, 33(17):7008–7016, 2021.
- [16] Stephen Wu, Yukiko Kondo, Masa-aki Kakimoto, Bin Yang, Hironao Yamada, Isao Kuwajima, Guillaume Lambard, Kenta Hongo, Yibin Xu, Junichiro Shiomi, et al. Machine-learning-assisted discovery of polymers with high thermal conductivity using a molecular design algorithm. *Npj Computational Materials*, 5(1):66, 2019.
- [17] Tu Le, V Chandana Epa, Frank R Burden, and David A Winkler. Quantitative structure–property relationship modeling of diverse materials properties. *Chemical reviews*, 112(5):2889–2919, 2012.
- [18] Tran Doan Huan, Arun Mannodi-Kanakkithodi, and Rampi Ramprasad. Accelerated materials property predictions and design using motif-based fingerprints. *Physical Review B*, 92(1):014106, 2015.
- [19] Hirotomo Moriwaki, Yu-Shi Tian, Norihito Kawashita, and Tatsuya Takagi. Mordred: a molecular descriptor calculator. *Journal of cheminformatics*, 10(1):1–14, 2018.

- [20] Christopher Kuenneth and Rampi Ramprasad. polyBERT: a chemical language model to enable fully machine-driven ultrafast polymer informatics. *Nature Communications*, 14(1):4099, 2023.
- [21] Changwen Xu, Yuyang Wang, and Amir Barati Farimani. TransPolymer: a transformer-based language model for polymer property predictions. *npj Computational Materials*, 9(1):64, 2023.
- [22] Jacob Devlin Ming-Wei Chang Kenton and Lee Kristina Toutanova. Bert: Pre-training of deep bidirectional transformers for language understanding. In *Proceedings of naacL-HLT*, volume 1, page 2, 2019.
- [23] Zhuang Liu, Wayne Lin, Ya Shi, and Jun Zhao. A robustly optimized bert pre-training approach with post-training. In *China National Conference on Chinese Computational Linguistics*, pages 471–484. Springer, 2021.
- [24] Tom Brown, Benjamin Mann, Nick Ryder, Melanie Subbiah, Jared D Kaplan, Prafulla Dhariwal, Arvind Neelakantan, Pranav Shyam, Girish Sastry, Amanda Askell, et al. Language models are few-shot learners. *Advances in neural information processing systems*, 33:1877–1901, 2020.
- [25] Matthew E Peters, Mark Neumann, Luke Zettlemoyer, and Wen-tau Yih. Dissecting contextual word embeddings: Architecture and representation. *arXiv preprint arXiv:1808.08949*, 2018.
- [26] Alexis Conneau and Guillaume Lample. Cross-lingual language model pretraining. *Advances in neural information processing systems*, 32, 2019.
- [27] Xiaomin Fang, Lihang Liu, Jieqiong Lei, Donglong He, Shanzhuo Zhang, Jingbo Zhou, Fan Wang, Hua Wu, and Haifeng Wang. Geometry-enhanced molecular representation learning for property prediction. *Nature Machine Intelligence*, 4(2):127–134, 2022.
- [28] Cong Shen, Jiawei Luo, and Kelin Xia. Molecular geometric deep learning. *Cell Reports Methods*, 3(11), 2023.
- [29] Zhaoning Yu and Hongyang Gao. Molecular graph representation learning via heterogeneous motif graph construction. 2021.
- [30] Yin Fang, Qiang Zhang, Haihong Yang, Xiang Zhuang, Shumin Deng, Wen Zhang, Ming Qin, Zhuo Chen, Xiaohui Fan, and Huajun Chen. Molecular contrastive learning with chemical element knowledge graph. In *Proceedings of the AAAI Conference on Artificial Intelligence*, volume 36, pages 3968–3976, 2022.
- [31] Yuyang Wang, Jianren Wang, Zhonglin Cao, and Amir Barati Farimani. Molecular contrastive learning of representations via graph neural networks. *Nature Machine Intelligence*, 4(3):279–287, 2022.
- [32] Minggang Zeng, Jatin Nitin Kumar, Zeng Zeng, Ramasamy Savitha, Vijay Ramaseshan Chandrasekhar, and Kedar Hippalgaonkar. Graph convolutional neural networks for polymers property prediction. *arXiv preprint arXiv:1811.06231*, 2018.
- [33] Rishi Gurnani, Christopher Kuenneth, Aubrey Toland, and Rampi Ramprasad. Polymer informatics at scale with multitask graph neural networks. *Chemistry of Materials*, 35(4):1560–1567, 2023.
- [34] Mustafa Hajij, Ghada Zamzmi, Theodore Papamarkou, Nina Miolane, Aldo Guzmán-Sáenz, Karthikeyan Natesan Ramamurthy, Tolga Birdal, Tamal K Dey, Soham Mukherjee, Shreyas N Samaga, et al. Topological deep learning: Going beyond graph data.
- [35] Cristian Bodnar. *Topological Deep Learning: Graphs, Complexes, Sheaves*. PhD thesis, 2023.
- [36] Mustafa Hajij, Kyle Istvan, and Ghada Zamzmi. Cell complex neural networks. *arXiv preprint arXiv:2010.00743*, 2020.
- [37] Felix Hensel, Michael Moor, and Bastian Rieck. A survey of topological machine learning methods. *Frontiers in Artificial Intelligence*, 4:681108, 2021.
- [38] Mathilde Papillon, Sophia Sanborn, Mustafa Hajij, and Nina Miolane. Architectures of topological deep learning: A survey on topological neural networks. *arXiv preprint arXiv:2304.10031*, 2023.
- [39] Cristian Bodnar, Francesco Di Giovanni, Benjamin Chamberlain, Pietro Liò, and Michael Bronstein. Neural sheaf diffusion: A topological perspective on heterophily and oversmoothing in gnns. *Advances in Neural Information Processing Systems*, 35:18527–18541, 2022.
- [40] Lorenzo Giusti, Claudio Battiloro, Lucia Testa, Paolo Di Lorenzo, Stefania Sardellitti, and Sergio Barbarossa. Cell attention networks. In *2023 International Joint Conference on Neural Networks (IJCNN)*, pages 1–8. IEEE, 2023.

- [41] Yifan Feng, Haoxuan You, Zizhao Zhang, Rongrong Ji, and Yue Gao. Hypergraph neural networks. In *Proceedings of the AAAI conference on artificial intelligence*, volume 33, pages 3558–3565, 2019.
- [42] Eun-Sol Kim, Woo Young Kang, Kyoung-Woon On, Yu-Jung Heo, and Byoung-Tak Zhang. Hypergraph attention networks for multimodal learning. In *Proceedings of the IEEE/CVF conference on computer vision and pattern recognition*, pages 14581–14590, 2020.
- [43] Song Bai, Feihu Zhang, and Philip HS Torr. Hypergraph convolution and hypergraph attention. *Pattern Recognition*, 110:107637, 2021.
- [44] Michael T Schaub, Jean-Baptiste Seby, Florian Frantzen, T Mitchell Roddenberry, Yu Zhu, and Santiago Segarra. Signal processing on simplicial complexes. In *Higher-Order Systems*, pages 301–328. Springer, 2022.
- [45] Jakob Hansen and Robert Ghrist. Toward a spectral theory of cellular sheaves. *Journal of Applied and Computational Topology*, 3:315–358, 2019.
- [46] Cristian Bodnar, Fabrizio Frasca, Yuguang Wang, Nina Otter, Guido F Montufar, Pietro Lio, and Michael Bronstein. Weisfeiler and leman go topological: Message passing simplicial networks. In *International Conference on Machine Learning*, pages 1026–1037. PMLR, 2021.
- [47] Kelin Xia and Guo-Wei Wei. Persistent homology analysis of protein structure, flexibility, and folding. *International journal for numerical methods in biomedical engineering*, 30(8):814–844, 2014.
- [48] Freyr Sverrisson, Jean Feydy, Bruno E Correia, and Michael M Bronstein. Fast end-to-end learning on protein surfaces. In *Proceedings of the IEEE/CVF Conference on Computer Vision and Pattern Recognition*, pages 15272–15281, 2021.
- [49] Zixuan Cang and Guo-Wei Wei. TopologyNet: Topology based deep convolutional and multi-task neural networks for biomolecular property predictions. *PLoS computational biology*, 13(7):e1005690, 2017.
- [50] Jiahui Chen, Yuchi Qiu, Rui Wang, and Guo-Wei Wei. Persistent laplacian projected omicron ba. 4 and ba. 5 to become new dominating variants. *Computers in Biology and Medicine*, 151:106262, 2022.
- [51] Patrick Reiser, Marlen Neubert, André Eberhard, Luca Torresi, Chen Zhou, Chen Shao, Houssam Metni, Clint van Hoesel, Henrik Schopmans, Timo Sommer, et al. Graph neural networks for materials science and chemistry. *Communications Materials*, 3(1):93, 2022.
- [52] Jacob Townsend, Cassie Putman Micucci, John H Hymel, Vasileios Maroulas, and Konstantinos D Vogiatzis. Representation of molecular structures with persistent homology for machine learning applications in chemistry. *Nature communications*, 11(1):3230, 2020.
- [53] T Mitchell Roddenberry, Nicholas Glaze, and Santiago Segarra. Principled simplicial neural networks for trajectory prediction. In *International Conference on Machine Learning*, pages 9020–9029. PMLR, 2021.
- [54] Maosheng Yang and Elvin Isufi. Convolutional learning on simplicial complexes. *arXiv preprint arXiv:2301.11163*, 2023.
- [55] Edelsbrunner, Letscher, and Zomorodian. Topological persistence and simplification. *Discrete & Computational Geometry*, 28:511–533, 2002.
- [56] Martin Dietrich Buhmann. Radial basis functions. *Acta numerica*, 9:1–38, 2000.
- [57] Shuangli Li, Jingbo Zhou, Tong Xu, Dejing Dou, and Hui Xiong. GeomGCL: Geometric graph contrastive learning for molecular property prediction. In *Proceedings of the AAAI conference on artificial intelligence*, volume 36, pages 4541–4549, 2022.
- [58] Dongkuan Xu, Wei Cheng, Dongsheng Luo, Haifeng Chen, and Xiang Zhang. Infogcl: Information-aware graph contrastive learning. *Advances in Neural Information Processing Systems*, 34:30414–30425, 2021.
- [59] Yonglong Tian, Chen Sun, Ben Poole, Dilip Krishnan, Cordelia Schmid, and Phillip Isola. What makes for good views for contrastive learning? *Advances in neural information processing systems*, 33:6827–6839, 2020.
- [60] Zhirong Wu, Yuanjun Xiong, Stella X Yu, and Dahua Lin. Unsupervised feature learning via non-parametric instance discrimination. In *Proceedings of the IEEE conference on computer vision and pattern recognition*, pages 3733–3742, 2018.
- [61] Kihyuk Sohn. Improved deep metric learning with multi-class n-pair loss objective. *Advances in neural information processing systems*, 29, 2016.

- [62] Ting Chen, Yizhou Sun, Yue Shi, and Liangjie Hong. On sampling strategies for neural network-based collaborative filtering. In *Proceedings of the 23rd ACM SIGKDD International Conference on Knowledge Discovery and Data Mining*, pages 767–776, 2017.
- [63] Deepak Kamal, Huan Tran, Chiho Kim, Yifei Wang, Lihua Chen, Yang Cao, V Roshan Joseph, and Rampi Ramprasad. Novel high voltage polymer insulators using computational and data-driven techniques. *The Journal of Chemical Physics*, 154(17), 2021.
- [64] Shinji Nagasawa, Eman Al-Naamani, and Akinori Saeki. Computer-aided screening of conjugated polymers for organic solar cell: classification by random forest. *The Journal of Physical Chemistry Letters*, 9(10):2639–2646, 2018.
- [65] Ye Hu, Dagmar Stumpfe, and Jürgen Bajorath. Computational exploration of molecular scaffolds in medicinal chemistry: Miniperspective. *Journal of medicinal chemistry*, 59(9):4062–4076, 2016.
- [66] David L Davies and Donald W Bouldin. A cluster separation measure. *IEEE transactions on pattern analysis and machine intelligence*, (2):224–227, 1979.

A Appendix / supplemental material

A.1 Proofs of corollaries

Lemma 1. For any pair of view (v_1, v_2) generated from Rip_r for prediction of a semantic label y that satisfies $I(v_1; y) = I(v_2; y) = I(\text{Rip}_r; y)$, the mutual information of the pair naturally has a lower bound:

$$I(v_1; v_2) \geq I(\text{Rip}_r; y)$$

Proof. because the fact that v_1, v_2 are functions of Rip_r , we have $I(\text{Rip}_r; y) = I(v_1; y) \leq I(v_1, v_2; y) \leq I(\text{Rip}_r; y)$, which implies:

$$I(\text{Rip}_r; y) = I(v_1; y) = I(v_1, v_2; y)$$

From the above Equation and $I(v_1, v_2; y) = I(v_1; y) + I(v_2; y | v_1)$, we know $I(v_2; y | v_1) = 0$. Thus, we have $I(v_1; v_2) = I(v_1; v_2) + I(v_2; y | v_1) = I(v_1, y; v_2) = I(v_2, y) + I(v_1, v_2 | y) \geq I(v_2, y) = I(\text{Rip}_r; y)$.

Proposition 1. (Optimal Augmented Views) For a downstream task T of prediction of a semantic label y , the optimal views, $(H_{r,k}^a)^*$, $(H_{r,k}^b)^*$, generated from the input simplicial complex Rip_r are the solutions to the following optimization problem:

$$(v_1^*, v_2^*) = \arg \min_{v_1, v_2} I(v_1; v_2) \quad (1)$$

subject to

$$I(v_1; y) = I(v_2; y) = I(\text{Rip}_r; y) \quad (2)$$

Proof. Because the optimal views $(H_{r,k}^a)^*$, $(H_{r,k}^b)^*$ retains all the information from the input simplicial complex Rip_r relevant to the label y , the Equation (2) holds for these views. Also, the shared information between the optimal views is only related to the label y , which means these views should be conditionally independent:

$$I((H_{r,k}^a)^*; (H_{r,k}^b)^* | y) = 0 \quad (3)$$

From the proof of Lemma 1, we know the Equation (3) implies $I((H_{r,k}^a)^*; (H_{r,k}^b)^*)$ reaches its lower bound $I(\text{Rip}_r; y)$. This proves that the optimal views $(H_{r,k}^a)^*$ and $(H_{r,k}^b)^*$ are solution of the optimal problem (1).

A.2 Supplementary figures and tables

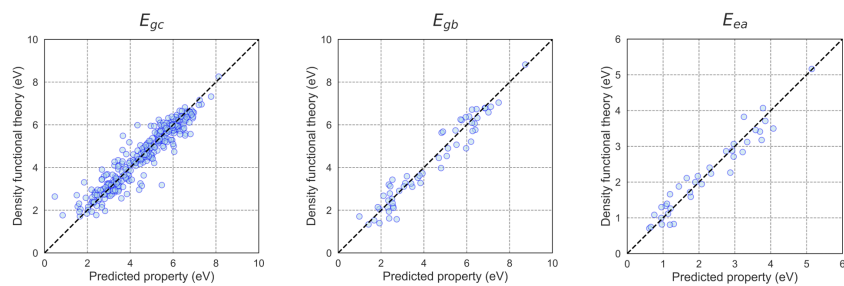


Figure 1: Scatter plots of predicted values by Mol-TDL for three datasets: E_{gc} , E_{gb} , E_{ea} . The dashed lines on diagonals stand for perfect regression.

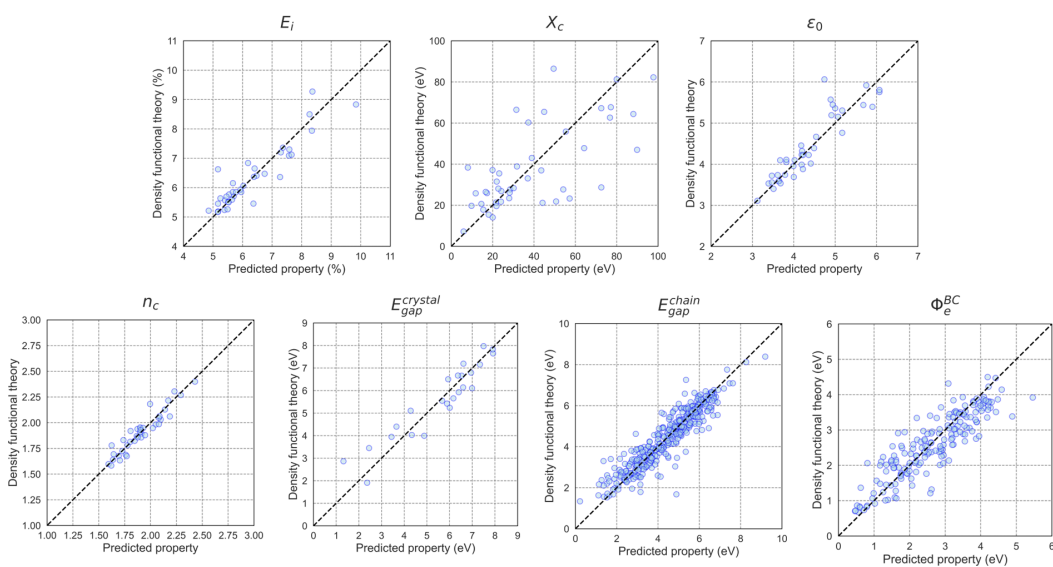


Figure 2: Scatter plots of predicted values by Mol-TDL for ten datasets: E_i , X_c , ϵ_0 , n_c , $E_{gap}^{crystal}$, E_{gap}^{chain} , Φ_e^{BC} . The dashed lines on diagonals stand for perfect regression.

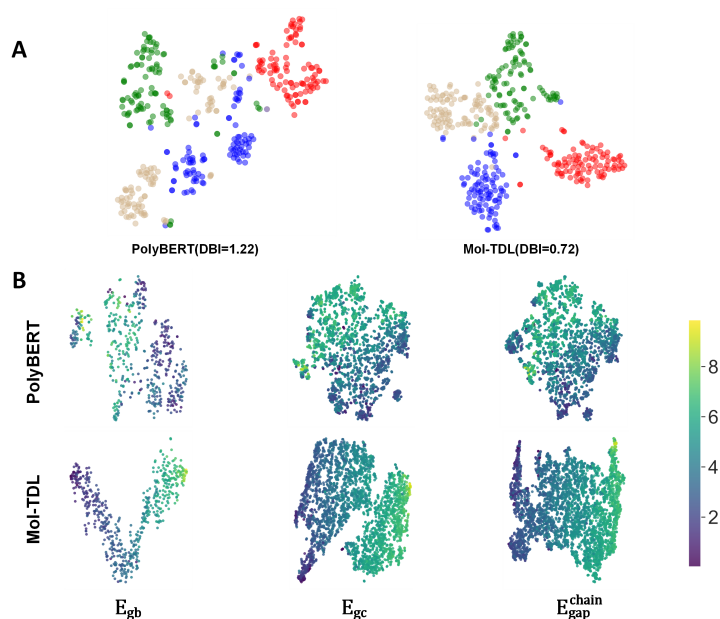


Figure 3: Visualization of the representations learned by different models. **A.** Visualization of Mol-TDL and polyBERT latent representations of different scaffolds (indicated by different colors). **B.** Visualization of Mol-TDL and polyBERT latent representations for E_{gb} , E_{gc} and E_{gap}^{chain} .

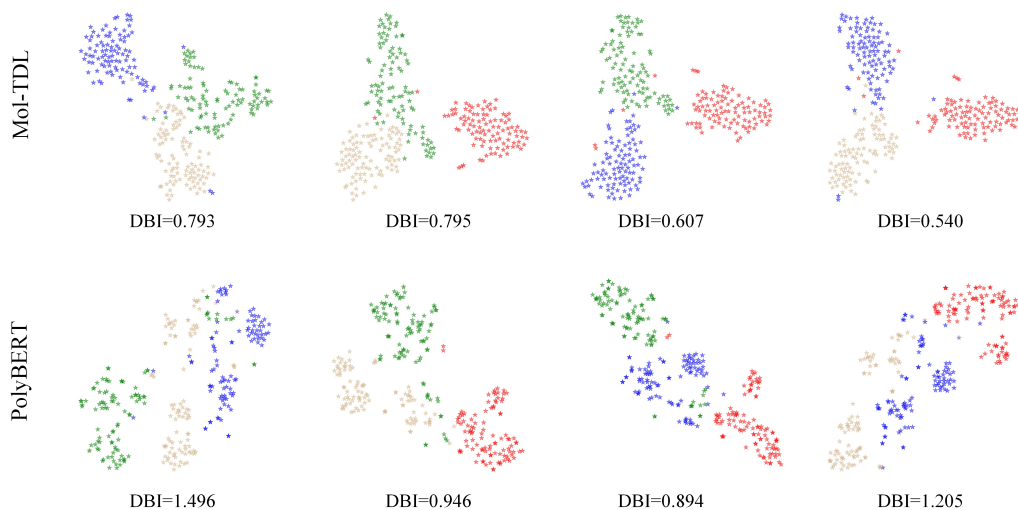


Figure 4: The t-SNE visualization results with Mol-TDL and PolyBERT. The number in bracket indicates DBI and the smaller the number, the better the clustering effect. The different colors indicate different scaffolds.

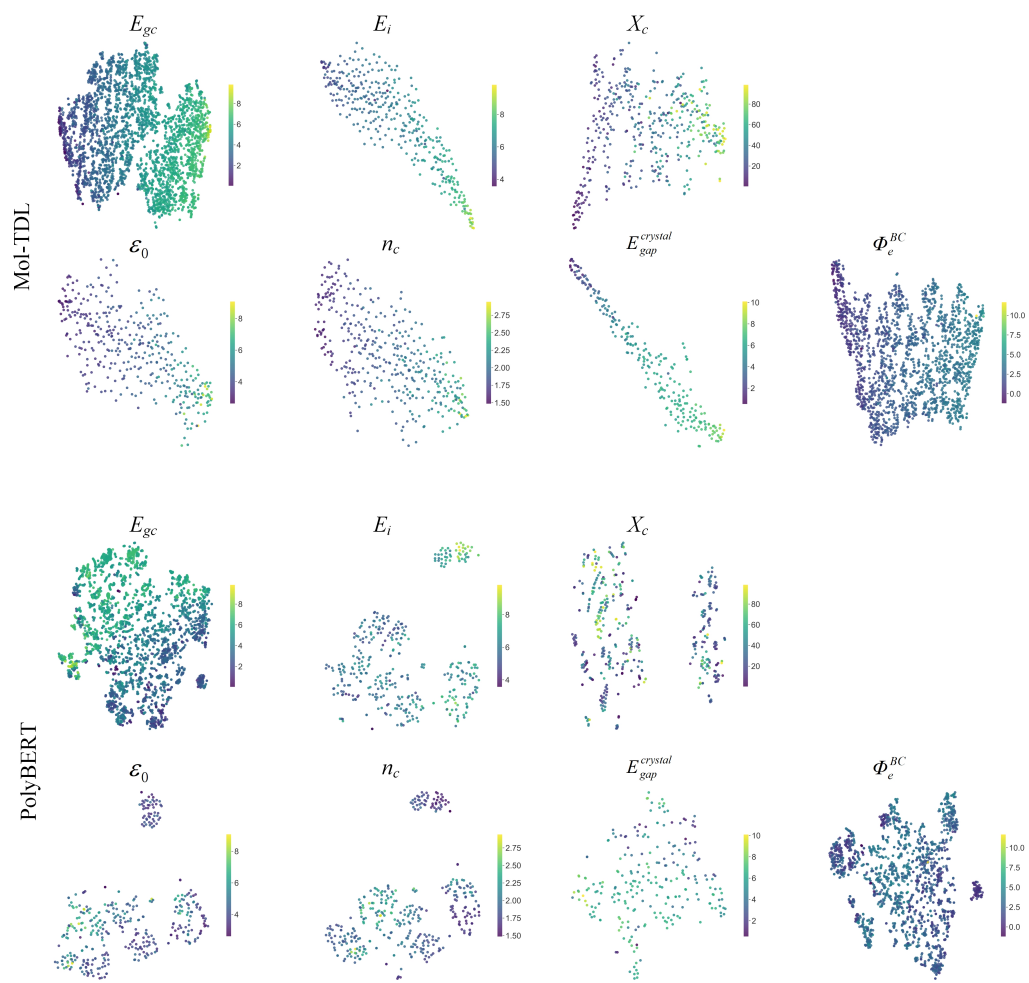


Figure 5: Distribution visualization of predicted polymer property of Mol-TDL and PolyBERT for the seven test sets.

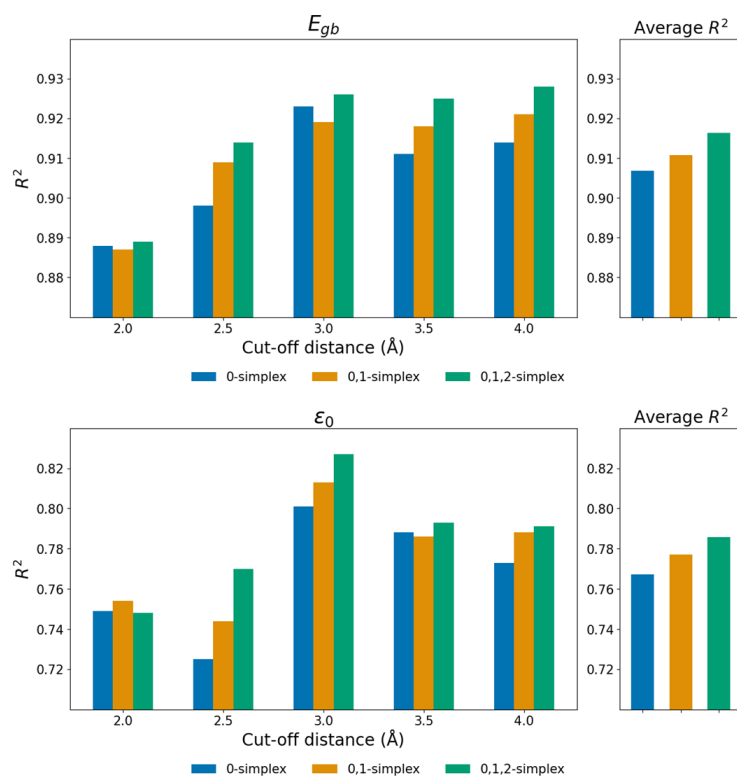


Figure 6: The performance of polymer property prediction based on the Vietoris–Rips complex at various cut-off distances and different combination of higher-order simplex features.

Table 1: Datasets for polymer property predictors

Datasets	Property	Units	Source	Data range	Polymers
E_{gc}	bandgap (chain)	eV	DFT	[0.02,9.86]	3390
E_{gb}	bandgap (bulk)	eV	DFT	[0.4,10.1]	561
E_{ea}	electron affinity	eV	DFT	[-0.39,5.17]	368
E_i	ionization energy	eV	DFT	[3.56,9.84]	370
X_c	crystallization tendency	%	DFT	[0.1,98.8]	432
ϵ_0	dielectric constant	1	DFT	[2.6,9.1]	382
n_c	refractive index	1	DFT	[1.48,2.95]	382
$E_{gap}^{crystal}$	crystal bandgap	eV	DFT	[0.5068,10.1137]	236
E_{gap}^{chain}	chain bandgap	eV	DFT	[0.071,9.8351]	4209
Φ_e^{BC}	charge injection barrier	eV	DFT	[-1.234,11.702]	1826
OPV_{Ave}	power conversion efficiency	1	DFT	[0.01,10.5]	1203
OPV_{Jsc}	short-circuit current density	mA/cm^2	DFT	[0.11,23.5]	1203
OPV_{Voc}	open-circuit voltage	V	DFT	[0.2,1.09]	1203
OPV_{Eg}	bandgap	eV	DFT	[1.0,2.4]	1203
OPV_{HOMO}	highest occupied molecular orbital	eV	DFT	[4.24,6.18]	1203
OPV_{LUMO}	lowest unoccupied molecular orbital	eV	DFT	[2.3,4.9]	1203

Table 2: The performance of polymer property prediction based on different interval molecular graph and different higher-order interactions (dataset: E_{gc}).

Simplex types	The cut-off distance					Average
	2.0 Å	2.5 Å	3.0 Å	3.5 Å	4.0 Å	
Metrics: R^2						
0-simplex	0.842 \pm 0.032	0.851 \pm 0.023	0.836 \pm 0.008	0.836 \pm 0.013	0.855 \pm 0.011	0.844 \pm 0.009
0,1-simplex	0.849 \pm 0.023	0.855 \pm 0.011	0.838 \pm 0.015	0.848 \pm 0.013	0.859 \pm 0.014	0.850 \pm 0.008
0,1,2-simplex	0.854 \pm 0.018	0.872 \pm 0.015	0.854 \pm 0.024	0.853 \pm 0.010	0.865 \pm 0.004	0.860 \pm 0.009
Metrics: $RMSE$						
0-simplex	0.585 \pm 0.061	0.568 \pm 0.044	0.598 \pm 0.014	0.597 \pm 0.024	0.562 \pm 0.021	0.582 \pm 0.016
0,1-simplex	0.572 \pm 0.044	0.562 \pm 0.022	0.594 \pm 0.028	0.575 \pm 0.025	0.554 \pm 0.028	0.572 \pm 0.015
0,1,2-simplex	0.564 \pm 0.034	0.527 \pm 0.030	0.562 \pm 0.048	0.566 \pm 0.020	0.543 \pm 0.009	0.552 \pm 0.017

Table 3: The performance of polymer property prediction based on different interval molecular graph and different higher-order interactions (dataset: E_{gb}).

Simplex types	The cut-off distance					Average
	2.0 Å	2.5Å	3.0Å	3.5Å	4.0Å	
Metrics: R^2						
0-simplex	0.888 \pm 0.005	0.898 \pm 0.021	0.923 \pm 0.008	0.911 \pm 0.006	0.914 \pm 0.006	0.907 \pm 0.014
0,1-simplex	0.887 \pm 0.028	0.909 \pm 0.006	0.919 \pm 0.013	0.918 \pm 0.008	0.921 \pm 0.011	0.911 \pm 0.014
0,1,2-simplex	0.889 \pm 0.019	0.914 \pm 0.009	0.926 \pm 0.009	0.925 \pm 0.007	0.928 \pm 0.012	0.916 \pm 0.016
Metrics: $RMSE$						
0-simplex	0.643 \pm 0.015	0.610 \pm 0.062	0.532 \pm 0.029	0.573 \pm 0.020	0.563 \pm 0.020	0.584 \pm 0.043
0,1-simplex	0.641 \pm 0.079	0.579 \pm 0.020	0.545 \pm 0.045	0.549 \pm 0.026	0.538 \pm 0.036	0.571 \pm 0.043
0,1,2-simplex	0.637 \pm 0.055	0.564 \pm 0.030	0.522 \pm 0.031	0.526 \pm 0.025	0.513 \pm 0.043	0.552 \pm 0.051

Table 4: The performance of polymer property prediction based on different interval molecular graph and different higher-order interactions (dataset: E_{ea}).

Simplex types	The cut-off distance					Average
	2.0 Å	2.5Å	3.0Å	3.5Å	4.0Å	
Metrics: R^2						
0-simplex	0.935 \pm 0.007	0.919 \pm 0.012	0.920 \pm 0.006	0.928 \pm 0.011	0.923 \pm 0.016	0.929 \pm 0.015
0,1-simplex	0.932 \pm 0.010	0.923 \pm 0.013	0.917 \pm 0.012	0.918 \pm 0.012	0.920 \pm 0.009	0.926 \pm 0.015
0,1,2-simplex	0.924 \pm 0.006	0.904 \pm 0.019	0.920 \pm 0.019	0.929 \pm 0.008	0.912 \pm 0.011	0.922 \pm 0.015
Metrics: $RMSE$						
0-simplex	0.246 \pm 0.021	0.330 \pm 0.025	0.330 \pm 0.012	0.312 \pm 0.023	0.323 \pm 0.034	0.308 \pm 0.036
0,1-simplex	0.253 \pm 0.025	0.324 \pm 0.026	0.334 \pm 0.024	0.332 \pm 0.025	0.330 \pm 0.018	0.315 \pm 0.035
0,1,2-simplex	0.276 \pm 0.016	0.359 \pm 0.035	0.328 \pm 0.042	0.310 \pm 0.019	0.345 \pm 0.022	0.324 \pm 0.032

Table 5: The performance of polymer property prediction based on different interval molecular graph and different higher-order interactions (dataset: E_i).

Simplex types	The cut-off distance					Average
	2.0 Å	2.5Å	3.0Å	3.5Å	4.0Å	
Metrics: R^2						
0-simplex	0.820 \pm 0.027	0.835 \pm 0.035	0.798 \pm 0.026	0.812 \pm 0.030	0.810 \pm 0.012	0.815 \pm 0.014
0,1-simplex	0.816 \pm 0.030	0.856 \pm 0.009	0.820 \pm 0.022	0.828 \pm 0.014	0.815 \pm 0.025	0.827 \pm 0.017
0,1,2-simplex	0.823 \pm 0.040	0.865 \pm 0.017	0.829 \pm 0.020	0.842 \pm 0.012	0.844 \pm 0.018	0.841 \pm 0.016
Metrics: $RMSE$						
0-simplex	0.485 \pm 0.036	0.463 \pm 0.048	0.514 \pm 0.034	0.495 \pm 0.043	0.499 \pm 0.016	0.491 \pm 0.019
0,1-simplex	0.490 \pm 0.040	0.434 \pm 0.014	0.485 \pm 0.030	0.475 \pm 0.020	0.492 \pm 0.033	0.475 \pm 0.024
0,1,2-simplex	0.479 \pm 0.057	0.420 \pm 0.027	0.473 \pm 0.028	0.456 \pm 0.018	0.452 \pm 0.026	0.456 \pm 0.023

Table 6: The performance of polymer property prediction based on different interval molecular graph and different higher-order interactions (dataset: X_c).

Simplex types	The cut-off distance					Average
	2.0 Å	2.5 Å	3.0 Å	3.5 Å	4.0 Å	
Metrics: R^2						
0-simplex	0.475 \pm 0.095	0.441 \pm 0.112	0.387 \pm 0.098	0.459 \pm 0.081	0.357 \pm 0.083	0.424 \pm 0.050
0,1-simplex	0.452 \pm 0.090	0.483 \pm 0.071	0.423 \pm 0.056	0.470 \pm 0.033	0.366 \pm 0.138	0.439 \pm 0.046
0,1,2-simplex	0.486 \pm 0.041	0.362 \pm 0.088	0.363 \pm 0.061	0.384 \pm 0.090	0.380 \pm 0.050	0.395 \pm 0.052
Metrics: $RMSE$						
0-simplex	17.675 \pm 1.670	18.227 \pm 1.904	19.120 \pm 1.526	17.963 \pm 1.319	19.594 \pm 1.265	18.516 \pm 0.810
0,1-simplex	18.076 \pm 1.484	17.569 \pm 1.227	18.577 \pm 0.908	17.820 \pm 0.563	19.387 \pm 2.176	18.286 \pm 0.720
0,1,2-simplex	17.545 \pm 0.698	19.511 \pm 1.317	19.525 \pm 0.928	19.173 \pm 1.379	19.262 \pm 0.773	19.003 \pm 0.830

Table 7: The performance of polymer property prediction based on different interval molecular graph and different higher-order interactions (dataset: ε_0).

Simplex types	The cut-off distance					Average
	2.0 Å	2.5 Å	3.0 Å	3.5 Å	4.0 Å	
Metrics: R^2						
0-simplex	0.749 \pm 0.011	0.725 \pm 0.024	0.801 \pm 0.018	0.788 \pm 0.007	0.773 \pm 0.009	0.767 \pm 0.030
0,1-simplex	0.754 \pm 0.006	0.744 \pm 0.025	0.813 \pm 0.011	0.786 \pm 0.020	0.788 \pm 0.015	0.777 \pm 0.028
0,1,2-simplex	0.748 \pm 0.042	0.770 \pm 0.025	0.827 \pm 0.028	0.793 \pm 0.020	0.791 \pm 0.015	0.786 \pm 0.029
Metrics: $RMSE$						
0-simplex	0.393 \pm 0.009	0.411 \pm 0.018	0.350 \pm 0.016	0.361 \pm 0.006	0.373 \pm 0.008	0.378 \pm 0.025
0,1-simplex	0.389 \pm 0.005	0.397 \pm 0.019	0.339 \pm 0.010	0.362 \pm 0.018	0.361 \pm 0.013	0.369 \pm 0.023
0,1,2-simplex	0.393 \pm 0.033	0.376 \pm 0.021	0.325 \pm 0.027	0.356 \pm 0.018	0.359 \pm 0.012	0.362 \pm 0.025

Table 8: The performance of polymer property prediction based on different interval molecular graph and different higher-order interactions (dataset: n_c).

Simplex types	The cut-off distance					Average
	2.0 Å	2.5 Å	3.0 Å	3.5 Å	4.0 Å	
Metrics: R^2						
0-simplex	0.869 \pm 0.013	0.876 \pm 0.015	0.892 \pm 0.006	0.886 \pm 0.006	0.893 \pm 0.010	0.883 \pm 0.011
0,1-simplex	0.878 \pm 0.009	0.861 \pm 0.023	0.889 \pm 0.009	0.881 \pm 0.019	0.894 \pm 0.017	0.881 \pm 0.013
0,1,2-simplex	0.899 \pm 0.013	0.873 \pm 0.019	0.895 \pm 0.011	0.882 \pm 0.012	0.894 \pm 0.012	0.889 \pm 0.011
Metrics: $RMSE$						
0-simplex	0.072 \pm 0.004	0.070 \pm 0.004	0.065 \pm 0.002	0.067 \pm 0.002	0.065 \pm 0.003	0.068 \pm 0.003
0,1-simplex	0.069 \pm 0.003	0.074 \pm 0.006	0.066 \pm 0.003	0.068 \pm 0.006	0.065 \pm 0.005	0.068 \pm 0.004
0,1,2-simplex	0.063 \pm 0.004	0.071 \pm 0.005	0.064 \pm 0.003	0.068 \pm 0.003	0.064 \pm 0.004	0.066 \pm 0.003

Table 9: The performance of polymer property prediction based on different interval molecular graph and different higher-order interactions (dataset: $E_{gap}^{crystal}$).

Simplex types	The cut-off distance					Average
	2.0 Å	2.5 Å	3.0 Å	3.5 Å	4.0 Å	
Metrics: R^2						
0-simplex	0.851 \pm 0.025	0.781 \pm 0.068	0.798 \pm 0.060	0.748 \pm 0.067	0.796 \pm 0.020	0.795 \pm 0.037
0,1-simplex	0.860 \pm 0.021	0.770 \pm 0.066	0.824 \pm 0.043	0.774 \pm 0.044	0.806 \pm 0.016	0.807 \pm 0.037
0,1,2-simplex	0.808 \pm 0.021	0.813 \pm 0.052	0.865 \pm 0.014	0.811 \pm 0.012	0.812 \pm 0.018	0.822 \pm 0.024
Metrics: $RMSE$						
0-simplex	0.688 \pm 0.059	0.828 \pm 0.137	0.797 \pm 0.115	0.892 \pm 0.114	0.807 \pm 0.041	0.802 \pm 0.074
0,1-simplex	0.667 \pm 0.050	0.849 \pm 0.128	0.745 \pm 0.090	0.848 \pm 0.082	0.787 \pm 0.033	0.779 \pm 0.077
0,1,2-simplex	0.783 \pm 0.044	0.767 \pm 0.116	0.656 \pm 0.035	0.777 \pm 0.024	0.775 \pm 0.038	0.752 \pm 0.054

Table 10: Comparison of performance of Mol-TDL models with or without pre-training process.

Datasets	Without pre-training		With pre-training	
	RMSE	R^2	RMSE	R^2
E_{gc}	0.516 \pm 0.013	0.878 \pm 0.006	0.510 \pm 0.012	0.881 \pm 0.006
E_{gb}	0.485 \pm 0.017	0.936 \pm 0.005	0.535 \pm 0.058	0.922 \pm 0.012
E_{ea}	0.276 \pm 0.008	0.934 \pm 0.003	0.263 \pm 0.013	0.944 \pm 0.005
E_i	0.464 \pm 0.030	0.835 \pm 0.021	0.417 \pm 0.021	0.867 \pm 0.013
X_c	16.448 \pm 1.130	0.547 \pm 0.063	15.862 \pm 0.825	0.579 \pm 0.045
ε_0	0.353 \pm 0.017	0.797 \pm 0.019	0.350 \pm 0.016	0.801 \pm 0.019
n_c	0.069 \pm 0.004	0.880 \pm 0.013	0.068 \pm 0.006	0.882 \pm 0.021
$E_{gap}^{crystal}$	0.608 \pm 0.034	0.884 \pm 0.013	0.567 \pm 0.057	0.899 \pm 0.020
E_{gap}^{chain}	0.539 \pm 0.012	0.863 \pm 0.006	0.587 \pm 0.010	0.837 \pm 0.006
Φ_e^{BC}	0.541 \pm 0.010	0.747 \pm 0.010	0.539 \pm 0.015	0.749 \pm 0.014